Secure Transmission Design for Aerial IRS Assisted Wireless Networks

Wenjing Wei, Xiaowei Pang, Jie Tang, *Senior Member, IEEE,* Nan Zhao, *Senior Member, IEEE*, Xianbin Wang, *Fellow, IEEE*, and Arumugam Nallanathan, *Fellow, IEEE*

***Abstract*—Combining intelligent reflecting surface (IRS) and unmanned aerial vehicle (UAV) offers a new degree of freedom to improve the coverage performance. However, it is more challenging to secure the air-ground transmission, due to the line-of-sight (LoS) links established by UAV. Since IRS is a promising solution for wireless environment reconfiguration, in this paper, we propose an aerial IRS-assisted secure transmission design in wireless networks. In particular, an access point (AP) equipped with a uniform planar array serves several single-antenna legitimate users in the presence of multiple single-antenna eavesdroppers, whose precise positions are unknown. An IRS is mounted on the UAV to help establish desired virtual LoS links between the AP and legitimate users, while ensuring their security. We aim to maximize the worst-case sum secrecy rate by jointly optimizing the hovering position of UAV, the transmit beamforming of AP and the phase shifts of IRS, subject to the requirement of minimum rate for legitimate users. To tackle this non-convex problem, we first decompose it into three subproblems, which are transformed into convex ones via successive convex approximation. An alternating algorithm is then proposed to solve them iteratively. Simulation results show the effectiveness of the proposed scheme and the security improvement by the joint optimization.**

***Index Terms*—Intelligent reflecting surface, unmanned aerial vehicle, physical layer security, joint beamforming optimization.**

I. Introduction

With the vigorous development of the sixth-generation (6G) wireless network, numerous novel wireless transmission technologies have been proposed. Among them, holographic multiple-input multiple-output surfaces (HMIMOS) [2] and intelligent reflecting surface (IRS) [3] have been expected to achieve an intelligent and reconfigurable paradigm for future wireless networks. Specially, IRS has been considered as a promising technology in the 6G networks to achieve high-quality wireless communications [4]. IRS is a man-made reconfigurable surface equipped with a large number of passive reflecting elements [5]. Through a smart controller, each element can tune the amplitude and/or phase of the electromagnetic wave independently to reconfigure the propagation environment [6]. Different from conventional active relays, IRS can passively reflect signals without self-interference in a full-duplex manner [7], which can dramatically improve the spectrum and energy efficiency. Thanks to its advantages, IRS has attracted a huge attention in various wireless scenarios and applications [8], such as employing IRSs to improve the coverage of networks [9], assist mobile edge computing [10], maximize energy efficiency [11], boost throughput [12] and enhance physical layer security (PLS) [13].

In terms of PLS, many different techniques have been developed by exploring various aspects of communication signal transmission and reception [14], such as the multi-antenna relaying [15], artificial noise [16], cooperative beamforming [17], *etc*. These methods can mitigate the eavesdropping channels and suppress the information received by eavesdroppers. Recently, IRS has been introduced to PLS for security enhancement through wireless environment reconfiguration [18]. Compared with the aforementioned methods, IRS is more cost effective, energy-efficient and easier to implement. Specifically, IRS can reconstruct the propagation environment by adaptively adjusting the reflecting elements to boost the desired signal received by the legitimate users while suppressing the eavesdropping channel quality. Thus, IRS-assisted secure transmission design has received increasing attentions [19]–[21]. In [19], Jiang *et al*. jointly optimized the multi-carrier beamforming of base station (BS) and the passive beamforming of IRS to maximize the sum secrecy rate. The artificial noise (AN) is incorporated with the beamforming by Hong *et al*. to enhance the PLS in [20], where the precoding matrix, the AN covariance matrix and the phase shifts of IRS were jointly optimized. Moreover, a deep reinforcement learning (DRL)-based approach was proposed by Yang *et al*. in [21] to improve the system secrecy rate in the IRS-aided networks.

On the other hand, thanks to its mobility and on-demand deployment, unmanned aerial vehicle (UAV) has been widely used in diverse fields, such as weather monitoring, emergency search and rescue, information broadcasting, aerial relaying, data collection [22]–[25], *etc*. With the onboard signal processing capability, it can act as aerial base stations (BSs) to improve the network coverage. Despite of the benefits provided by UAV, there are still many challenges in UAV-aided wireless networks. In particular, UAV's broadcasting channels are more susceptible to potential eavesdroppers due to the line-of-sight (LoS) channel between UAV and any ground users.

W. Wei, X. Pang and N. Zhao are with the School of Information and Communication Engineering, Dalian University of Technology, Dalian 116024, China. (e-mail: weiwj@mail.dlut.edu.cn, xiaoweipang00@mail.dlut.edu.cn, zhaonan@dlut.edu.cn).

J. Tang is with the School of Electronic and Information Engineering, South China University of Technology, Guangzhou, China. (e-mail: eejtang@scut.edu.cn).

X. Wang is with the Department of Electrical and Computer Engineering, Western University, London N6A 5B9, Canada. (e-mail: xianbin.wang@uwo.ca).

A. Nallanathan is with the School of Electronic Engineering and Computer Science, Queen Mary University of London, London E1 4NS, U.K. (e-mail: a. Nallanathan@qmul.ac.uk).

Part of this work is submitted to IEEE ICC'23 [1].

Hence, achieving security in UAV-enabled networks becomes a critical issue. Artificial jamming has been intensively studied in the UAV assisted secure transmission to improve the PLS. In [26], the optimal jamming power and UAV placement were jointly investigated by Liu *et al*. to achieve the highest secrecy rate. In [27], Zhong *et al*. jointly optimized the UAVs' trajectories and the transmit and jamming power to maximize the average secrecy rate. Chen *et al*. in [28] investigated that artificial jamming can be jointly optimized with the UAV's transmit beamforming to achieve the confidential transmission with all the legitimate users.

More recently, the appealing advantages of UAV and IRS motivate the researchers to combine them to further release their potentials [29]. Depending on where the IRS is deployed, there are mainly two methods to combine IRS and UAV. One is IRS-assisted UAV networks, where the IRS is installed on the facades of buildings or indoor walls/ceilings to reflect the electromagnetic wave between the UAV and ground nodes. Wei *et al*. jointly optimized the UAV's trajectory, the IRS scheduling, and the resource allocation to maximize the system sun rate [30]. Besides, several IRSs were employed to assist UAV communication by Ge *et al*. to maximize the received power at the user, where the trajectory and active beamforming of UAV and the passive beamforming were jointly designed [31]. Furthermore, Pang *et al*. proposed a secure IRS-assisted UAV transmission scheme in [13], and jointly optimized the trajectory of UAV, and the active and passive beamforming to maximize the average secrecy rate. The other one is mounting IRS on the UAV to achieve intelligent reflection from the sky. Aerial IRS can realize omni-directional reflection and reach the desired destination via only one reflection [32]. Specifically, an IRS-UAV network scheme was proposed by Su *et al*. in [33], where the transmit beamforming of BS, the passive beamforming of IRS and UAV's trajectory were designed to maximize the spectrum efficiency and the energy efficiency. Niu *et al*. in [34] jointly designed the deployment and the phase shifts of aerial IRS to maximize the secrecy rate.

Motivated by combined advantages of combining IRS and UAV, in this paper, we employ aerial IRS to enhance the performance of wireless security. Different from the existing works on aerial IRS assisted secure communication considering one legitimate user and a single eavesdropper with perfect location information, we focus on the case of multiple eavesdroppers with imperfect location information and aim to maximize the worst-case sum secrecy rate while guaranteeing the minimum rate requirement of the legitimate users. The main contributions of this paper are summarized as follows.

- We propose an aerial IRS aided secure communication scheme, where the IRS is mounted on a UAV to help the AP transmit confidential data to multiple legitimate users in the presence of multiple eavesdroppers. To enhance the security, the hovering position of UAV, the transmit beamforming of AP and the phase-shift matrix of IRS are jointly optimized to maximize the worst-case sum secrecy rate.
- To guarantee a favorable propagation environment, the LoS probability ensured by the UAV is utilized when designing the UAV placement. In addition, to make it more practical, we assume that the prefect location information of the eavesdroppers cannot be acquired. Each eavesdropper is assumed to locate in a circular estimated region with the center and radius.
- Due to the non-convexity of the original optimization problem, it is first decomposed into three subproblems, which are then approximated into convex ones by successive convex approximation (SCA) and semidefinite relaxation (SDR). An iterative algorithm is developed to solve the approximate convex problems in an alternating manner until convergence.

The rest of this paper is structured as follows. Section II introduces the system and channel models. The joint optimization problem is formulated in Section III. In Section IV, the problem is decomposed into three subproblems, and then an iterative algorithm is proposed. Section V presents the simulation results. Finally, Section VI concludes the work.

Notation: $\mathbb{C}^{M\times N}$ represents the dimension of complex matrices. $\mathbb{H}^M$ denotes the $M \times M$ Hermitian matrices. $\mathbf{1}_M$ denotes the $M \times 1$ all-ones vector. $\mathbf{X}^T$ and $\mathbf{X}^H$ refer to the transpose and the conjugate transpose operations of the matrix $\mathbf{X}$, respectively. $\mathbf{X} \succeq 0$ indicates that $\mathbf{X}$ is a positive semidefinite matrix. The Euclidean norm of a vector is denoted as $\|\mathbf{x}\|$ and the absolute value of a complex scalar is denoted as $|x|$. $\mathrm{diag}(\mathbf{x})$ stands for the diagonal matrix of $\mathbf{x}$. $\mathrm{Diag}(\mathbf{X})$ stands for a vector whose elements are extracted from the diagonal elements of $\mathbf{X}$. $\mathrm{Tr}(\mathbf{X})$ and $\mathrm{Rank}(\mathbf{X})$ indicate the trace and rank of $\mathbf{X}$, respectively. $\mathcal{CN}(\mathbf{n}, \mathbf{\Sigma})$ denotes the circularly symmetric complex Gaussian (CSCG) distribution with mean vector $\mathbf{n}$ and covariance matrix $\mathbf{\Sigma}$. $\otimes$ denotes the Kronecker product. For a complex number a, $\arg(a)$ represents its phase. $\bigtriangledown_x$ represents the gradient of the variable x and $[x]^+ = \max\{0, x\}$. Superscript (t) denotes the iteration index of the optimization variables.

II. System Model

As shown in Fig. 1, we consider an aerial IRS-assisted secure wireless network consisting of a multi-antenna AP, K single-antenna legitimate users, E single-antenna eavesdroppers[1] with uncertain positions and an IRS on the UAV.

Assume that the direct links from the AP to users are blocked by obstacles in the urban environment. To solve this issue, the IRS carried by UAV can establish virtual LoS links for them while guaranteeing the security.

We consider a 3D Cartesian coordinate system with the AP located at the origin. The ground users are on the x-y plane, where the coordinates of legitimate users and eavesdroppers are denoted by $\mathbf{q}_k = [x_k, y_k, 0]^T, \forall k \in \mathcal{K}, \mathcal{K} = \{1, ..., K\}$ and $\mathbf{q}_e = [x_e, y_e, 0]^T, \forall e \in \mathcal{E}, \mathcal{E} = \{1, ..., E\}$, respectively. The precise positions of eavesdroppers are unknown. Instead, the UAV can estimate their approximate positions through aerial photography target detection [35] and share the information with the AP. As such, we assume that each eavesdropper's estimated region centered at $\hat{\mathbf{q}}_e = [\hat{x}_e, \hat{y}_e, 0]^T, \forall e \in \mathcal{E}$, with

[1]Herein, we consider that the eavesdroppers are active or serve as licensed users but have no authority to access the confidential information.

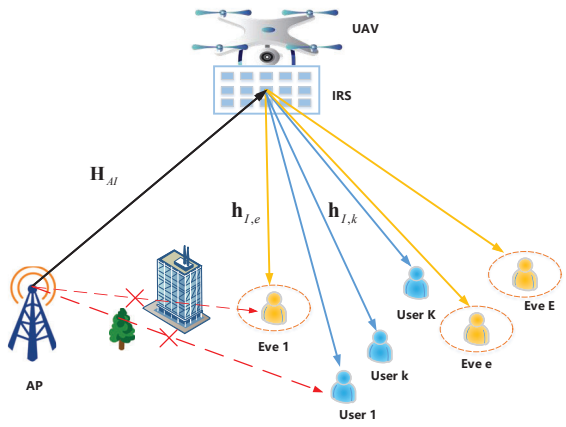

Fig. 1. Aerial IRS-enabled secure wireless network.

radius $\epsilon_e \geq \|\hat{\mathbf{q}}_e - \mathbf{q}_e\|$ known to the UAV. The bottom-left element of IRS located at $\mathbf{q}_I = [x_I, y_I, z_I]^T$ is regarded as the reference point. In the system, we adopt the classic model of LoS probability, which can be given by

$$P_{LoS} = \frac{1}{1 + \alpha \exp\left(-\beta\left[\theta_{u,i} - \alpha\right]\right)}, \tag{1}$$

where the constants α and β depend on the specific environment, and $\theta_{u,i}$ is the elevation angle towards the UAV from the ground user's perspective [36]. In order to ensure LoS for the communication links, the constraint that the LoS probability is larger than a threshold will be introduced to the optimization problem of UAV position. Thus, we can consider the LoS-dominant channel model for air-ground communications due to the high LoS probability ensured by the high-altitude deployment of UAV. The channel power gain from AP to IRS can be expressed as

$$\beta_{AI} = \beta_0 d_{AI}^{-2}, \tag{2}$$

where β_0 denotes the channel gain at the reference distance d_0= 1 m, and $d_{AI} = \|\mathbf{q}_I\|$ represents the distance from AP to IRS. Similarly, the channel power gain from IRS to any ground node i can be expressed as

$$\beta_{I,i} = \beta_0 d_{I,i}^{-2}, \quad \forall i \in \{\mathcal{K}, \mathcal{E}\}, \tag{3}$$

where $d_{I,i} = \sqrt{\|\mathbf{q}_I - \mathbf{q}_i\|^2}$ represents the distance from IRS to the ground user i.

We first define a steering function for a uniform planar array (UPA) given its size N, element spacing d and directional cosine ω, which can be given by

$$\mathbf{g}(N, d, \omega) = \left[1, e^{-j\frac{2\pi}{\lambda}d\omega}, ..., e^{-j\frac{2\pi}{\lambda}(N-1)d\omega}\right], \tag{4}$$

where λ is the carrier wavelength.

The AP is assumed to be equipped with a UPA with $N_t = N_y N_z$ antennas, where N_y and N_z denote the number of antennas along the y-axis and z-axis, respectively. d_1 and d_2 respectively denote the antenna separation in the y-axis and z-axis. Thus, the transmit array response with respect to the azimuth and elevation angle-of-departures (AoDs) from AP to IRS, i.e., ϕ_A and η_A, can be given as

$$\begin{aligned}\mathbf{a}(\phi_A, \eta_A) =& \mathbf{g}(N_y, d_1, \sin(\phi_A)\sin(\eta_A)) \otimes \\ & \mathbf{g}(N_z, d_2, \cos(\phi_A)).\end{aligned} \tag{5}$$

The IRS consists of a UPA with $M = M_x M_y$ passive reflecting elements, where M_x and M_y denote the number of elements along the x-axis and y-axis, respectively. With the element spacing of IRS denoted by d_x and d_y, respectively, the array response vector of IRS can be expressed as

$$\begin{aligned}\mathbf{a}(\phi_n, \eta_n) =& \mathbf{g}(M_x, d_x, \sin(\phi_n)\cos(\eta_n)) \otimes \\ & \mathbf{g}(M_y, d_y, \sin(\phi_n)\sin(\eta_n)), \forall n \in \{O, \mathcal{K}, \mathcal{E}\},\end{aligned} \tag{6}$$

where n represents a specific ground node, e.g., the AP (O), a legitimate user or an eavesdropper. ϕ_n and η_n respectively denote the zenith and azimuth angles-of-arrival (AoAs)/AoDs of the signal from the specific ground node to IRS.

Considering the existing channel estimation techniques for IRS-assisted communications [37], [38], all the channel state information (CSI) is assumed to be available in the legitimate network in this paper. Base on (5) and (6), the channel matrix from AP to IRS $\mathbf{H}_{AI} \in \mathbb{C}^{M \times N_t}$ can be expressed as

$$\mathbf{H}_{AI} = \sqrt{\beta_{AI}} e^{-j\frac{2\pi}{\lambda}d_{AI}} \mathbf{a}^T(\phi_O, \eta_O)\mathbf{a}(\phi_A, \eta_A). \tag{7}$$

Similarly, the channel from IRS to a specific ground user i $\mathbf{h}_{I,i} \in \mathbb{C}^{1 \times M}$ can be given by

$$\mathbf{h}_{I,i}^H = \sqrt{\beta_{I,i}} e^{-j\frac{2\pi}{\lambda}d_{I,i}} \mathbf{a}(\phi_i, \eta_i), \quad \forall i \in \{\mathcal{K}, \mathcal{E}\}. \tag{8}$$

Accordingly, the received signal at the ground user i can be denoted as

$$y_i = \mathbf{h}_{I,i}^H \mathbf{\Phi} \mathbf{H}_{AI} \sum_{l \in \mathcal{K}} \mathbf{w}_l s_l + n_i, \quad \forall i \in \{\mathcal{K}, \mathcal{E}\}, \tag{9}$$

where $s_l \in \mathbb{C}$ is the signal transmitted by AP to the kth legitimate user with $\mathbb{E}\left[|s_l|^2\right] = 1$, and $\mathbf{w}_l \in \mathbb{C}^{N_t \times 1}$ is the corresponding beamforming vector. The phase-shift matrix of IRS is given by $\mathbf{\Phi} = \text{diag}\left[e^{j\theta_1}, ..., e^{j\theta_M}\right]$, where θ_m is the controllable phase shift introduced by the mth reflecting element. In addition, $n_i \sim \mathcal{CN}(0, \sigma_i^2)$ represents the additive white Gaussian noise (AWGN) at the ground user i.

Based on the signal model in (9), the achievable rate of the kth legitimate user can be expressed as

$$R_k = \log_2\left(1 + \frac{\left|\mathbf{h}_{I,k}^H \mathbf{\Phi} \mathbf{H}_{AI} \mathbf{w}_k\right|^2}{\sigma_k^2 + \sum\limits_{i \in \mathcal{K} \setminus \{k\}} \left|\mathbf{h}_{I,k}^H \mathbf{\Phi} \mathbf{H}_{AI} \mathbf{w}_i\right|^2}\right), \forall k \in \mathcal{K}. \tag{10}$$

The achievable rate of the eth eavesdropper to decode the signal of the kth legitimate user can be given by

$$R_{e,k} = \log_2\left(1 + \frac{|\mathbf{h}_{I,e}^H \mathbf{\Phi} \mathbf{H}_{AI} \mathbf{w}_k|^2}{\sigma_e^2 + \sum\limits_{i \in \mathcal{K} \setminus \{k\}} |\mathbf{h}_{I,e}^H \mathbf{\Phi} \mathbf{H}_{AI} \mathbf{w}_i|^2)}\right), \forall k, e. \tag{11}$$

III. Problem Formulation

In this section, we formulate the optimization problem of the hovering position $\mathbf{q}_I$ of UAV, the transmit beamforming $\mathbf{w}_k$ of AP and the phase shift matrix $\mathbf{\Phi}$ of IRS. Our goal is to maximize the sum secrecy rate while guaranteeing the minimum rate of legitimate users.

To ensure the secure transmission, we maximize the worst-case sum secrecy rate with the maximum achievable eavesdropping rate considered. We consider LoS channels between IRS and the eavesdroppers, as they are very close to the legitimate users. In this case, an upper bound of the eavesdropping rate is considered when calculating the secrecy rate. To confirm the worst-case secrecy rate, Proposition 1 is presented to find the maximum achievable eavesdropping rate within the uncertainty region.

Proposition 1. The eavesdropping rate monotonically decreases with respect to the distance from IRS to the eavesdropper.

Proof: For convenience, we first define a function as

$$f(x) = \log_2\left(1 + \frac{a}{x^2 + b}\right), \tag{12}$$

where $x \geq 0$, and a and b are positive constants. Its gradient can be calculated as

$$\nabla_x f(x) = \left(\frac{\frac{-2ax}{(x^2+b)^2}}{1 + \frac{2}{x^2+b}}\right). \tag{13}$$

We can observe from (13) that $\nabla_x f(x)$ is always negative. Based on (11), the eavesdropping rate of the eth eavesdropper with respect to the variable $d_{I,e}$ can be rewritten as

$$R_{e,k} = \log_2\left(1 + \frac{A}{d_{I,e}^2 + B}\right), \tag{14}$$

where A and B are two positive constants. As observed, the expression (14) has the same form as (12). As such, its gradient is always negative. Therefore, we can conclude that the eavesdropping rate monotonically decreases with respect to the distance from IRS to the eavesdropper. ■

Then, considering the linear algebra and applying the triangular inequality [39], we have

$$\begin{aligned} \|\mathbf{q}_I - \mathbf{q}_e\| &\geq \left|\|\mathbf{q}_I - \hat{\mathbf{q}}_e\| - \|\hat{\mathbf{q}}_e - \mathbf{q}_e\|\right| \\ &\geq \left|\|\mathbf{q}_I - \hat{\mathbf{q}}_e\| - \varepsilon_e\right|. \end{aligned} \tag{15}$$

The closest distance from IRS to the eth eavesdropper can be expressed as

$$\hat{d}_{I,e} = \left|\|\mathbf{q}_I - \hat{\mathbf{q}}_e\| - \epsilon_e\right|, \quad \forall e \in \mathcal{E}. \tag{16}$$

Thus, the channel from IRS to the eth eavesdropper corresponding to the closest distance can be denoted as

$$\hat{\mathbf{h}}_{I,e}^H = \sqrt{\hat{\beta}_{I,e}} e^{-j\frac{2\pi}{\lambda}\hat{d}_{I,e}} \hat{\mathbf{a}}\left(\hat{\phi}_e, \hat{\eta}_e\right), \quad \forall e \in \mathcal{E}, \tag{17}$$

where $\sqrt{\hat{\beta}_{I,e}}$ can be obtained by substituting (17) into (3), $\hat{\phi}_e$, $\hat{\eta}_e$ and $\hat{\mathbf{a}}\left(\hat{\phi}_e, \hat{\eta}_e\right)$ can be obtained by utilizing the center position of each eavesdropper's estimated region.

According to the above derivation, the maximum achievable rate of the eth eavesdropper within the uncertainty region R_e, can be given by

$$R_{e,k}^{max} = \log_2\left(1 + \frac{\left|\hat{\mathbf{h}}_{I,e}^H \mathbf{\Phi} \mathbf{H}_{AI} \mathbf{w}_k\right|^2}{\sigma_e^2 + \sum\limits_{i \in \mathcal{K}\setminus\{k\}} \left|\hat{\mathbf{h}}_{I,e}^H \mathbf{\Phi} \mathbf{H}_{AI} \mathbf{w}_i\right|^2}\right), \ \forall k, e. \tag{18}$$

Hence, the worst-case achievable secrecy rate at the kth legitimate user can be obtained by

$$R_{s,k} = \left[R_k - \max_{e \in \mathcal{E}}\left\{R_{e,k}^{max}\right\}\right]^+, \quad \forall k \in \mathcal{K}, \forall e \in \mathcal{E}, \tag{19}$$

where $[x]^+ \triangleq \max\{x, 0\}$. Actually, $R_k - \max_{e\in\mathcal{E}}\{R_{e,k}^{max}\}$ can be always guaranteed to be non-negative because it can be made zero by adjusting the transmit power to zero if it is negative. Thus, $[\cdot]^+$ will be omitted in the rest of this paper.

According to the obtained worst-case achievable secrecy rate, the joint optimization problem can be formulated as [40]

$$\begin{aligned} \max_{\mathbf{q}_I, \mathbf{w}_k, \mathbf{\Phi}} \ & \sum_{k \in \mathcal{K}} R_{s,k} \\ s.t. \ & \mathrm{C1}: P_{LoS} \geq \varepsilon_{LoS}, \\ & \mathrm{C2}: \mathbf{q}_{Imin} \leq \mathbf{q}_I \leq \mathbf{q}_{Imax}, \\ & \mathrm{C3}: \sum_{k \in \mathcal{K}} \|\mathbf{w}_k\|^2 \leq P, \\ & \mathrm{C4}: |e^{j\theta_m}| = 1, \ \ 1 \leq m \leq M, \\ & \mathrm{C5}: R_k \geq r_k, \ \ \forall k \in \mathcal{K}. \end{aligned} \tag{20}$$

In order to ensure the reliable connection of air-ground links, the constraint C1 is to restrict the channels from AP to IRS and those from IRS to the legitimate users to LoS by making the LoS probability larger than a threshold ε_{LoS}. The range of UAV's hovering position is limited by the constraint C2, with $\mathbf{q}_{Imin}$ and $\mathbf{q}_{Imax}$ denoting the nearest and farthest positions of UAV from AP, respectively. In the constraint C3, the maximum transmit power of AP is denoted as P . The constraint C5 ensures that the achievable rate of the kth legitimate user is not lower than the given threshold r_k.

It can be observed that (20) is non-convex because the optimization variables are highly coupled in the objective function. To tackle this challenge, we decompose it into three sub-problems, and solve them iteratively in the next section.

IV. Joint Optimization for Secrecy Rate Maximization

In this section, the alternating optimization (AO) is adopted to obtain the solution to (20) by alternately optimizing one variable while fixing the other two. For the first subproblem of UAV position, we apply SCA and approximate it to solve. For the non-convex subproblems of the transmit beamforming and the phase shifts, we resort to SDR and SCA to tackle them, respectively. Finally, the detailed algorithm is summarized.

A. Optimization of UAV Placement

According to the model of LoS probability, the constraint $P_{LoS} \geq \varepsilon_{LoS}$ leads to $\sin(\theta_{u,i}) \geq \sin(\theta(\varepsilon_{LoS}))$, where

$$\sin(\theta_{u,i}) = \frac{d_{u,i}}{z_I}, \tag{21a}$$

$$\sin(\theta(\varepsilon_{LoS})) = \sin\left(\alpha + \frac{\ln\frac{\alpha\varepsilon_{LoS}}{1-\varepsilon_{LoS}}}{\beta}\right) \triangleq D. \tag{21b}$$

Thus, we have the constraint $Dd_{u,i} \leq z_I$ to ensure the high LoS probability.

Given the transmit beamforming vectors $\mathbf{w}_k$ and the phase-shift matrix $\mathbf{\Phi}$, the optimization problem of UAV position can be separated from (20) as

$$\begin{aligned} \max_{\mathbf{q}_I} \ & \sum_{k\in\mathcal{K}} R_{s,k} \\ s.t. \ & \overline{\mathrm{C1}} : \max(Dd_{AI} - z_I, Dd_{I,k} - z_I) \leq 0, \\ & \mathrm{C2} : \mathbf{q}_{Imin} \leq \mathbf{q}_I \leq \mathbf{q}_{Imax}, \\ & \mathrm{C5} : R_k \geq r_k, \ \forall k \in \mathcal{K}, \end{aligned} \tag{22}$$

which is non-convex with respect to the variable of UAV position $\mathbf{q}_I$. Specifically, the achievable rate of the kth legitimate user and the eth eavesdropper can be respectively rewritten as

$$R_k = \log_2\left(1 + \frac{A_k}{d_{AI}^2 d_{I,k}^2 + \sum\limits_{i\in\mathcal{K}\setminus\{k\}} A_i}\right), \ \forall k \in \mathcal{K}, \tag{23a}$$

$$R_{e,k}^{max} = \log_2\left(1 + \frac{A_{ek}}{d_{AI}^2 \hat{d}_{I,e}^2 + \sum\limits_{i\in\mathcal{K}\setminus\{k\}} A_{ei}}\right), \ \forall e \in \mathcal{E}, \tag{23b}$$

where

$$A_k = \frac{\beta_0^2 \mathbf{a}_k \mathbf{\Phi} \mathbf{a}_I^H \mathbf{a}_{N_t} \mathbf{w}_k \mathbf{w}_k^H \mathbf{a}_{N_t}^H \mathbf{a}_I \mathbf{\Phi}^H \mathbf{a}_k^H}{\sigma_k^2}, \tag{24a}$$

$$A_{ek} = \frac{\beta_0^2 \hat{\mathbf{a}}_e \mathbf{\Phi} \mathbf{a}_I^H \mathbf{a}_{N_t} \mathbf{w}_k \mathbf{w}_k^H \mathbf{a}_{N_t}^H \mathbf{a}_I \mathbf{\Phi}^H \hat{\mathbf{a}}_e^H}{\sigma_e^2}. \tag{24b}$$

To tackle the non-convex problem (22), we first deal with R_k and $R_{e,k}^{max}$ separately. For R_k, we introduce slack variables U, V_k and S_k, which satisfy

$$d_{AI} \leq U, \ d_{I,k} \leq V_k, \ UV_k \leq e^{S_k}, \ \forall k \in \mathcal{K}. \tag{25}$$

Then, we can construct a global underestimator for the achievable rate of the kth legitimate user given by

$$\begin{aligned} R_k &\geq \log_2\left(1 + \frac{A_k}{U^2 V_k^2 + \sum\limits_{i\in\mathcal{K}\setminus\{k\}} A_i}\right) \\ &\geq \log_2\left(1 + \frac{A_k}{e^{2S_k} + \sum\limits_{i\in\mathcal{K}\setminus\{k\}} A_i}\right) \\ &= \log_2\left(\sum_{k\in\mathcal{K}} A_k + e^{2S_k}\right) - \log_2\left(\sum_{i\in\mathcal{K}\setminus\{k\}} A_i + e^{2S_k}\right). \end{aligned} \tag{26}$$

Moreover, by utilizing the first-order Taylor expansions of $\log_2\left(\sum\limits_{k\in\mathcal{K}} A_k + e^{2S_k}\right)$ at any feasible point $S_{0k}^{(t)}$, the global underestimator for the achievable rate of the kth legitimate user can be converted into a concave counterpart as

$$\begin{aligned} R_k \geq & \log_2\left(\sum_{k\in\mathcal{K}} A_k + e^{2S_k}\right) - \log_2\left(\sum_{i\in\mathcal{K}\setminus\{k\}} A_i + e^{2S_{0k}^{(t)}}\right) \\ & + \frac{2e^{2S_{0k}^{(t)}}}{\ln 2\left(\sum\limits_{k\in\mathcal{K}} A_k + e^{2S_{0k}^{(t)}}\right)}\left(S_k - S_{0k}^{(t)}\right) \\ \triangleq & \ \tilde{R}_k, \ \ \forall k \in \mathcal{K}. \end{aligned} \tag{27}$$

Furthermore, slack variables u, v_e and T_e are introduced to deal with $R_{e,k}^{max}$, which satisfy

$$u \leq d_{AI}, \ v_e \leq \hat{d}_{I,e}, \ e^{T_e} \leq uv_e, \ \forall e \in \mathcal{E}. \tag{28}$$

Thus, the global underestimator for $-R_{e,k}^{max}$ can be expressed as

$$\begin{aligned} -R_{e,k}^{max} &\geq -\log_2\left(1 + \frac{A_{ek}}{u^2 v_e^2 + \sum\limits_{i\in\mathcal{K}\setminus\{k\}} A_{ei}}\right) \\ &\geq -\log_2\left(1 + \frac{A_{ek}}{e^{2T_e} + \sum\limits_{i\in\mathcal{K}\setminus\{k\}} A_{ei}}\right) \\ &= -\log_2\left(\sum_{k\in\mathcal{K}} A_{ek} + e^{2T_e}\right) + \log_2\left(\sum_{i\in\mathcal{K}\setminus\{k\}} A_{ei} + e^{2T_e}\right). \end{aligned} \tag{29}$$

To deal with the only remaining non-concavity in the expression of $-R_{e,k}^{max}$, we apply the first-order Taylor expansion on $\log_2\left(\sum\limits_{i\in\mathcal{K}\setminus\{k\}} A_{ei} + e^{2T_e}\right)$, and have

$$\begin{aligned} -R_{e,k}^{max} \geq & -\log_2\left(\sum_{k\in\mathcal{K}} A_{ek} + e^{2T_{0e}^{(t)}}\right) + \log_2\left(\sum_{i\in\mathcal{K}\setminus\{k\}} A_{ei} + e^{2T_e}\right) \\ & + \frac{2e^{2T_{0e}^{(t)}}}{\ln 2\left(\sum\limits_{i\in\mathcal{K}\setminus\{k\}} A_{ei} + e^{2T_{0e}^{(t)}}\right)}\left(T_e - T_{0e}^{(t)}\right) \\ \triangleq & -\tilde{R}_{e,k}, \ \forall k \in \mathcal{K}, e \in \mathcal{E}. \end{aligned} \tag{30}$$

By employing the lower bound of the objective function, the only remaining non-convexity of the problem (22) are the inequalities about slack variables, which will be converted into convex constraints through Lemma 1.

Lemma 1: The inequalities about slack variables can be transformed into convex constraints as

$$d_{AI}^2 - \widetilde{U}^2 \leq 0, \tag{31a}$$

$$d_{I,k}^2 - \widetilde{V}_k^2 \leq 0, \tag{31b}$$

$$\widetilde{\ln}(UV_k) - S_k \leq 0, \ \ \forall k \in \mathcal{K} \tag{31c}$$

$$u^2 - \tilde{d}_{AI}^2 \leq 0, \tag{31d}$$

$$v_e^2 - \tilde{d}_{I,e}^2 \leq 0. \tag{31e}$$

Proof: Note that the first-order Taylor approximation of a convex/concave function can provide a global under/upper estimator. Hence, with the given local points $U_0^{(t)}$, $V_{0k}^{(t)}$ and $\mathbf{q}_{I0}^{(t)}$ in the t-th iteration, we have

$$U^2 \geq \left[U_0^{(t)}\right]^2 + 2U_0^{(t)}\left(U - U_0^{(t)}\right) \triangleq \widetilde{U}^2, \tag{32a}$$

$$V_k^2 \geq \left[V_{0k}^{(t)}\right]^2 + 2V_{0k}^{(t)}\left(V_k - V_{0k}^{(t)}\right) \triangleq \widetilde{V}_k^2, \tag{32b}$$

$$\ln\left(UV_k\right) \leq \ln\left(U_0^{(t)}\right) + \frac{1}{U_0^{(t)}}\left(U - U_0^{(t)}\right) + \ln\left(V_{0k}^{(t)}\right) + \frac{1}{V_{0k}^{(t)}}\left(V - V_{0k}^{(t)}\right) \triangleq \widetilde{\ln}(UV_k),\ \forall k \in \mathcal{K}, \tag{32c}$$

$$d_{AI}^2 \geq \left\|\mathbf{q}_{I0}^{(t)}\right\|^2 + 2\left\|\mathbf{q}_{I0}^{(t)}\right\|^T\left(\|\mathbf{q}_I\| - \left\|\mathbf{q}_{I0}^{(t)}\right\|\right) \triangleq \tilde{d}_{AI}^2, \tag{32d}$$

$$\hat{d}_{I,e}^2 \geq \left\|\mathbf{q}_{I0}^{(t)} - \hat{\mathbf{q}}_e\right\|^2 + 2\left\|\mathbf{q}_{I0}^{(t)} - \hat{\mathbf{q}}_e\right\|^T\left(\|\mathbf{q}_I\| - \left\|\mathbf{q}_{I0}^{(t)}\right\|\right) - 2R_e\left\|\mathbf{q}_I - \hat{\mathbf{q}}_e\right\| + \varepsilon_e^2 \triangleq \tilde{d}_{I,e}^2,\ \forall e \in \mathcal{E}. \tag{32e}$$

According to (26), we have $d_{AI}^2 - U^2 \leq 0$. By substituting U^2 with its first-order Taylor approximation, (31a) can be obtained. Similarly, (31b)$\sim$ (31e) can be easily proved. ■

In addition, to deal with $e^{T_e} \leq uv_e$, we take the logarithm on both sides of the expression, and have

$$T_e - \log(u) - \log(v_e) \leq 0. \tag{33}$$

As a result, the problem (22) can be recasted into a convex problem as

$$\begin{aligned}
\max_{\substack{\mathbf{q}_I, U, V_k, \\ S_k, u, v_e, T_e}} \ & \sum_{k\in\mathcal{K}}\left(\tilde{R}_k - \max_{e\in\mathcal{E}}\{\tilde{R}_{e,k}\}\right) \\
s.t.\ \ & \mathrm{C1}: \max\left(Dd_{AI} - z_I, Dd_{I,k} - z_I\right) \leq 0, \\
& \mathrm{C2}: \mathbf{q}_{Imin} \leq \mathbf{q}_I \leq \mathbf{q}_{Imax}, \\
& \mathrm{C5}: \tilde{R}_k \geq r_k,\ \ \forall k \in \mathcal{K} \\
& \mathrm{C6a}: d_{AI}^2 - \widetilde{U}^2 \leq 0, \\
& \mathrm{C6b}: d_{I,k}^2 - \widetilde{V}_k^2 \leq 0, \\
& \mathrm{C6c}: \widetilde{\ln}(UV_k) - S_k \leq 0, \\
& \mathrm{C7a}: u^2 - \tilde{d}_{AI}^2 \leq 0, \\
& \mathrm{C7b}: v_e^2 - \tilde{d}_{I,e}^2 \leq 0, \\
& \mathrm{C7c}: T_e - \log(u) - \log(v_e) \leq 0,
\end{aligned} \tag{34}$$

which can be solved efficiently by standard solvers, such as CVX.

B. Optimization of Transmit Beamforming

Then, with the optimized UAV position $\mathbf{q}_I$ and the given phase-shift matrix $\mathbf{\Phi}$, the optimization problem of $\mathbf{w}_k$ can be formulated as

$$\begin{aligned}
\min_{\mathbf{w}_k} \ & -\sum_{k\in\mathcal{K}} R_{s,k} \\
s.t.\ \ & \mathrm{C3}: \sum_{k\in\mathcal{K}}\|\mathbf{w}_k\|^2 \leq P, \\
& \mathrm{C5}: R_k \geq r_k,\ \ \forall k \in \mathcal{K}.
\end{aligned} \tag{35}$$

However, the optimization problem is not convex with respect to $\mathbf{w}_k$. Thus, we rewrite (35) as a rank-constrained semidefinite programming (SDP) problem. With $\mathbf{W}_k \triangleq \mathbf{w}_k\mathbf{w}_k^H$, the problem (35) can be recasted as

$$\begin{aligned}
\min_{\mathbf{W}_k \in \mathbb{H}^{N_t}} \ & -\sum_{k\in\mathcal{K}}\left(\hat{R}_k - \max_{e\in\mathcal{E}}\{\hat{R}_{e,k}\}\right) \\
s.t.\ \ & \mathrm{C3}: \sum_{k\in\mathcal{K}}\mathrm{Tr}\left(\mathbf{W}_k\right) \leq P, \\
& \mathrm{C5}: \hat{R}_k \geq r_k,\ \ \forall k \in \mathcal{K} \\
& \mathrm{C8}: \mathbf{W}_k \succeq 0,\ \ \forall k \in \mathcal{K} \\
& \mathrm{C9}: \mathrm{Rank}(\mathbf{W}_k) \leq 1,\ \ \forall k \in \mathcal{K},
\end{aligned} \tag{36}$$

where

$$\hat{R}_k = \log_2\left(1 + \frac{\mathrm{Tr}\left(\mathbf{M}_k\mathbf{W}_k\right)}{\sigma_k^2 + \sum\limits_{i\in\mathcal{K}\setminus\{k\}}\mathrm{Tr}\left(\mathbf{M}_k\mathbf{W}_i\right)}\right), \tag{37a}$$

$$\hat{R}_{e,k} = \log_2\left(1 + \frac{\mathrm{Tr}\left(\mathbf{M}_e\mathbf{W}_k\right)}{\sigma_e^2 + \sum\limits_{i\in\mathcal{K}\setminus\{k\}}\mathrm{Tr}\left(\mathbf{M}_e\mathbf{W}_i\right)}\right). \tag{37b}$$

In (37), we have

$$\mathbf{M}_k = \mathbf{H}_{AI}^H\mathbf{\Phi}\mathbf{h}_{I,k}\mathbf{h}_{I,k}^H\mathbf{\Phi}\mathbf{H}_{AI},\ \ \forall k \in \mathcal{K} \tag{38a}$$

$$\mathbf{M}_e = \mathbf{H}_{AI}^H\mathbf{\Phi}\hat{\mathbf{h}}_{I,e}\mathbf{h}_{I,e}^H\mathbf{\Phi}\mathbf{H}_{AI},\ \ \forall e \in \mathcal{E}. \tag{38b}$$

Note that the constraints $\mathbf{W}_k \succeq 0$, $\mathbf{W}_k \in \mathbb{H}^{N_t}$ and $\mathrm{Rank}(\mathbf{W}_k) \leq 1$ are introduced to guarantee that $\mathbf{W}_k \triangleq \mathbf{w}_k\mathbf{w}_k^H$ still holds after optimizing $\mathbf{W}_k$.

This problem is intractable due to the non-convex objective function, for which we can apply SCA to make it convex based on Lemma 2.

Lemma 2: The objective function has a convex upper bound by utilizing the corresponding first-order Taylor approximation.

Proof: First, we rewrite the objective function in the form of difference of convex (d.c.) functions, i.e., $-\hat{R}_k = L_k - F_k$ and $\hat{R}_{e,k} = L_e - F_e$, where

$$L_k = -\log_2\left(\sigma_k^2 + \sum_{i\in\mathcal{K}}\mathrm{Tr}\left(\mathbf{W}_i\mathbf{M}_k\right)\right), \tag{39a}$$

$$F_k = -\log_2\left(\sigma_k^2 + \sum_{i\in\mathcal{K}\setminus\{k\}}\mathrm{Tr}\left(\mathbf{W}_i\mathbf{M}_k\right)\right), \forall k \in \mathcal{K}, \tag{39b}$$

$$L_e = \log_2\left(\sigma_e^2 + \sum_{i\in\mathcal{K}}\mathrm{Tr}\left(\mathbf{W}_i\mathbf{M}_e\right)\right), \tag{39c}$$

$$F_e = \log_2\left(\sigma_e^2 + \sum_{i\in\mathcal{K}\setminus\{k\}}\mathrm{Tr}\left(\mathbf{W}_i\mathbf{M}_e\right)\right), \forall e \in \mathcal{E}. \tag{39d}$$

It can be observed that the functions L_k and F_k are convex in terms of $\mathbf{W}_k$, while the functions L_e and F_e are concave. To facilitate the SCA, we construct a global lower bound for F_k and a global upper bound for L_e. In particular, for any

feasible point $\mathbf{W}^{(t)}$, a lower bound of the function F_k is given by its first-order Taylor approximation as

$$F_k(\mathbf{W}) \geq F_k\left(\mathbf{W}^{(t)}\right) + \mathrm{Tr}\left(\nabla^H_{\mathbf{W}_k} F_k\left(\mathbf{W}^{(t)}\right)\left(\mathbf{W}_k - \mathbf{W}_k^{(t)}\right)\right). \quad (40)$$

Similarly, an upper bound of the function N_e can be obtained by

$$L_e(\mathbf{W}) \leq L_e\left(\mathbf{W}^{(t)}\right) + \mathrm{Tr}\left(\nabla^H_{\mathbf{W}_k} L_e\left(\mathbf{W}^{(t)}\right)\left(\mathbf{W}_k - \mathbf{W}_k^{(t)}\right)\right), \quad (41)$$

where the gradients of F_k and L_e with respect to $\mathbf{W}_k$ can be expressed as

$$\nabla_{\mathbf{W}_k} F_k(\mathbf{W}) = -\frac{1}{\ln 2}\sum_{j\neq k}\frac{\mathbf{M}_j}{\sigma_j^2 + \sum\limits_{j\in\mathcal{K}\setminus\{j\}}\mathrm{Tr}(\mathbf{W}_i\mathbf{M}_j)}, \quad (42a)$$

$$\nabla_{\mathbf{W}_k} L_e(\mathbf{W}) = -\frac{1}{\ln 2}\sum_{k\in\mathcal{K}}\frac{\mathbf{M}_e}{\sigma_e^2 + \sum\limits_{k\in\mathcal{K}}\mathrm{Tr}(\mathbf{W}_i\mathbf{M}_e)}. \quad (42b)$$

Then, by substituting $F_k(\mathbf{W})$ and $L_e(\mathbf{W})$ with their respective first-order Taylor approximations, the objective function has its convex upper bound. This completes the proof. ■

Since the constraint C9 is difficult to solve, we adopt the SDR to relax it. As a result, the optimization problem (36) can be reduced to

$$\begin{aligned}\min_{\mathbf{W}_k\in\mathbb{H}^{N_t}} \ & \sum_{k\in\mathcal{K}}\Big(L_k - \mathrm{Tr}\left(\nabla^H_{\mathbf{W}_k}F_k\left(\mathbf{W}^{(t)}\right)\mathbf{W}_k\right) \\ & + \max_{e\in\mathcal{E}}\left\{\mathrm{Tr}\left(\nabla^H_{\mathbf{W}_k}L_e\left(\mathbf{W}^{(t)}\right)\mathbf{W}_k\right) - F_e\right\}\Big) \\ s.t.\ & \mathrm{C3}: \sum_{k\in\mathcal{K}}\mathrm{Tr}(\mathbf{W}_k) \leq P, \\ & \mathrm{C5}: L_k - F_k\left(\mathbf{W}^{(t)}\right) \\ & -\mathrm{Tr}\left(\nabla^H_{\mathbf{W}_k}F_k\left(\mathbf{W}^{(t)}\right)\left(\mathbf{W}_k - \mathbf{W}_k^{(t)}\right)\right) \leq -r_k, \\ & \mathrm{C8}: \mathbf{W}_k \succeq 0, \ \ \forall k\in\mathcal{K}.\end{aligned} \quad (43)$$

This relaxed problem (43) is convex with respect to $\mathbf{W}_k$, which can be solved efficiently. According to the results in [41], the optimal solution to (43) always satisfies the rank constraint, i.e., $\mathrm{Rank}(\mathbf{W}_k) \leq 1$. Therefore, the optimal beamforming vector $\mathbf{w}_k^*$ can be always recovered from $\mathbf{W}_k^*$ by applying the Cholesky decomposition.

C. Optimization of IRS Passive Beamforming

With the UAV position $\mathbf{q}_I$ and the transmit beamforming vectors $\mathbf{w}_k$ obtained by solving the abovementioned subproblems, the phase-shift subproblem can be expressed as

$$\begin{aligned}\min_{\theta_m} \ & -\sum_{k\in\mathcal{K}} R_{s,k} \\ s.t.\ & \mathrm{C4}: |e^{j\theta_m}| = 1, \ \ 1\leq m\leq M, \\ & \mathrm{C5}: R_k \geq r_k, \ \ \forall k\in\mathcal{K}.\end{aligned} \quad (44)$$

Let $\mathbf{v} = [v_1, ..., v_M]^T$, where $v_m = e^{j\theta_m}$, $\forall m \in M$. Then, the constraints in C4 can be equivalent to $|v_m| = 1$.

Let $\mathbf{N}_k = \mathrm{diag}(\mathbf{h}_{\mathrm{I},\mathrm{k}}^{\mathrm{H}})\mathbf{H}_{\mathrm{AI}}$, and we have

$$\begin{aligned}\left|\mathbf{h}_{I,k}^H\mathbf{\Phi}\mathbf{H}_{AI}\mathbf{w}_k\right|^2 &= \mathbf{v}^T\mathbf{N}_k\mathbf{W}_k\mathbf{N}_k^H\left(\mathbf{v}^T\right)^H \\ &= \mathrm{Tr}\left(\mathbf{N}_k\mathbf{W}_k\mathbf{N}_k^H\left(\mathbf{v}^H\right)^T\mathbf{v}^T\right).\end{aligned} \quad (45)$$

Then, to facilitate the SDP, we define $\mathbf{V} \triangleq \mathbf{v}\mathbf{v}^H$, and the problem (44) can be recast as

$$\begin{aligned}\min_{\mathbf{V}\in\mathbb{H}^M} \ & -\sum_{k\in\mathcal{K}}\left(\bar{R}_k - \max_{e\in\mathcal{E}}\{\bar{R}_{e,k}\}\right) \\ s.t.\ & \mathrm{C5}: \bar{R}_k \geq r_k, \ \ \forall k\in\mathcal{K}, \\ & \mathrm{C10}: \mathrm{Diag}(\mathbf{V}) = \mathbf{1}_M, \ \ \mathrm{C11}: \mathbf{V}\succeq\mathbf{0}, \\ & \mathrm{C12}: \mathrm{Rank}(\mathbf{V}) = 1,\end{aligned} \quad (46)$$

where $\mathbf{V}\in\mathbb{H}^M$, and C11 and C12 are introduced to guarantee that $\mathbf{V} \triangleq \mathbf{v}\mathbf{v}^H$ holds after optimization. In addition, the constraint C10 is introduced to guarantee the unit modulus constraint when recovering $\mathbf{v}$ from $\mathbf{V}$. $\bar{R}_k$ and $\bar{R}_{e,k}$ can be denoted as

$$\hat{R}_k = \log_2\left(1 + \frac{\mathrm{Tr}\left(\mathbf{N}_k\mathbf{W}_k\mathbf{N}_k^H\mathbf{V}^T\right)}{\sigma_k^2 + \sum\limits_{i\in\mathcal{K}\setminus\{k\}}\mathrm{Tr}\left(\mathbf{N}_k\mathbf{W}_i\mathbf{N}_k^H\mathbf{V}^T\right)}\right), \quad (47a)$$

$$\hat{R}_{e,k} = \log_2\left(1 + \frac{\mathrm{Tr}\left(\mathbf{N}_e\mathbf{W}_k\mathbf{N}_e^H\mathbf{V}^T\right)}{\sigma_e^2 + \sum\limits_{i\in\mathcal{K}\setminus\{k\}}\mathrm{Tr}\left(\mathbf{N}_e\mathbf{W}_i\mathbf{N}_e^H\mathbf{V}^T\right)}\right). \quad (47b)$$

The objective function is non-convex. Similar to the operations on $\mathbf{W}_k$, we rewrite the objective function in the form of d.c. functions, i.e., $-\bar{R}_k = l_k - f_k$ and $\bar{R}_{e,k} = l_e - f_e$, where

$$l_k = -\log_2\left(\sigma_k^2 + \sum_{i\in\mathcal{K}}\mathrm{Tr}\left(\mathbf{N}_k\mathbf{W}_i\mathbf{N}_k^H\mathbf{V}^T\right)\right), \quad (48a)$$

$$f_k = -\log_2\left(\sigma_k^2 + \sum_{i\in\mathcal{K}\setminus\{k\}}\mathrm{Tr}\left(\mathbf{N}_k\mathbf{W}_i\mathbf{N}_k^H\mathbf{V}^T\right)\right), \quad (48b)$$

$$l_e = \log_2\left(\sigma_e^2 + \sum_{i\in\mathcal{K}}\mathrm{Tr}\left(\mathbf{N}_e\mathbf{W}_i\mathbf{N}_e^H\mathbf{V}^T\right)\right), \quad (48c)$$

$$f_e = \log_2\left(\sigma_e^2 + \sum_{i\in\mathcal{K}\setminus\{k\}}\mathrm{Tr}\left(\mathbf{N}_e\mathbf{W}_i\mathbf{N}_e^H\mathbf{V}^T\right)\right). \quad (48d)$$

We adopt a similar method as that in Section IV-B to tackle the d.c. objective function. In particular, for any feasible point $\mathbf{V}^{(t)}$, a lower bound of f_k and an upper bound of l_e can be respectively obtained as

$$f_k(\mathbf{V}) \geq f_k\left(\mathbf{V}^{(t)}\right) + \mathrm{Tr}\left(\nabla^H_{\mathbf{V}} f_k\left(\mathbf{V}^{(t)}\right)\left(\mathbf{V} - \mathbf{V}^{(t)}\right)\right), \quad (49a)$$

$$l_e(\mathbf{V}) \leq l_e\left(\mathbf{V}^{(t)}\right) + \mathrm{Tr}\left(\nabla^H_{\mathbf{V}} l_e\left(\mathbf{V}^{(t)}\right)\left(\mathbf{V} - \mathbf{V}^{(t)}\right)\right), \quad (49b)$$

where $\nabla_{\mathbf{V}} f_k$ and $\nabla_{\mathbf{V}} l_e$ can be expressed as

$$\nabla_{\mathbf{V}} f_k = -\frac{1}{\ln 2}\frac{\mathbf{N}_k\sum_{i\in K\setminus\{k\}}\mathbf{W}_i\mathbf{N}_k^H}{\sigma_k^2 + \sum_{i\in\mathcal{K}\setminus\{k\}}\mathrm{Tr}\left(\mathbf{N}_k\mathbf{W}_i\mathbf{N}_k^H\mathbf{V}^T\right)}, \quad (50a)$$

$$\nabla_{\mathbf{V}} l_e = -\frac{1}{\ln 2}\frac{\mathbf{N}_e\left(\sum_{k\in K}\mathbf{W}_k\right)\mathbf{N}_e^H}{\sigma_e^2 + \sum_{k\in\mathcal{K}}\mathrm{Tr}\left(\mathbf{N}_e\mathbf{W}_k\mathbf{N}_e^H\mathbf{V}^T\right)}. \quad (50b)$$

Since the rank-one constraint is non-convex, we adopt SDR and omit the rank constraint C12. Thus, the problem (46) can

be recasted as

$$\begin{aligned}\min_{\mathbf{V}\in\mathbb{H}^M}\ & \sum_{k\in\mathcal{K}}\left(l_k-\mathrm{Tr}\left(\nabla_{\mathbf{V}}^H f_k\left(\mathbf{V}^{(t)}\right)\mathbf{V}\right)\right.\\ & \left.+\max_{e\in\mathcal{E}}\left\{\mathrm{Tr}\left(\nabla_{\mathbf{V}}^H l_e\left(\mathbf{V}^{(t)}\right)\mathbf{V}\right)-f_e\right\}\right)\\ s.t.\ & \mathrm{C2}: l_k-f_k\left(\mathbf{V}^{(t)}\right)\\ & -\mathrm{Tr}\left(\nabla_{\mathbf{V}}^H f_k\left(\mathbf{V}^{(t)}\right)\left(\mathbf{V}-\mathbf{V}^{(t)}\right)\right)\leq -r_k,\forall k,\\ & \mathrm{C10}: \mathrm{Diag}(\mathbf{V})=\mathbf{1}_M,\\ & \mathrm{C11}: \mathbf{V}\succeq\mathbf{0},\end{aligned}\tag{51}$$

which can be efficiently solved by existing optimization tools.

However, different from the transmit beamforming problem (43), the relaxed problem (51) generally obtains a solution with the rank larger than one. Thus, a rank-one solution needs to be obtained from the optimal higher-rank solution to the problem (51). First, by performing the eigenvalue decomposition of $\mathbf{V}$, we have $\mathbf{V}=\mathbf{G}\mathbf{\Lambda}\mathbf{G}^H$, where $\mathbf{G}=[e_1,...,e_M]$ and $\mathbf{\Lambda}=\mathrm{diag}(\lambda_1,...,\lambda_2)$ are a unitary matrix and a diagonal matrix, respectively. Then, we construct $\bar{\mathbf{v}}=\mathbf{G}\mathbf{\Lambda}^{\mathbf{1/2}}\mathbf{r}$, where $\mathbf{r}$ is a CSCG vector with $\mathbf{r}\sim\mathcal{CN}(\mathbf{0},\mathbf{I}_M)$. With independently generated Gaussian random vectors $\mathbf{r}$, the optimal $\bar{\mathbf{v}}$ can be obtained by substituting $\bar{\mathbf{V}}=\bar{\mathbf{v}}\bar{\mathbf{v}}^H$ into the problem (51) to minimize it. Finally, $\mathbf{v}$ can be recovered by $\mathbf{v}=e^{iarg(\bar{\mathbf{v}})}$. It has been proved in [42] that such an approach can obtain a $\frac{\pi}{4}$-approximation of the optimal objective value of the original problem.

D. Overall Algorithm

To maximize the sum secrecy rate, we solve the three sub-problems alternately until convergence. In each iteration, the solution to each sub-problem is updated by solving an approximate problem transformed from a non-convex one. The detailed AO algorithm to solve the problem (20) is summarized in Algorithm 1[2]

In Algorithm 1, an iterative algorithm is proposed to obtain a high-quality suboptimal solution to the sum secrecy rate maximization problem by alternately optimizing the three sub-problems. Specifically, for these three non-convex sub-problems (22), (35) and (44), we solve their approximate convex ones (34), (43) and (51) instead. The objective function obtained in each iteration serves as a lower bound of the original problem (20) and the objective value is non-decreasing with iterations. Through iteratively solving these sub-problems, we can monotonically tighten the lower bound. According to the proof in [43], Algorithm 1 can be guaranteed to converge to at least a local suboptimal solution, the details of which are omitted here. Furthermore, the computational complexity of the proposed algorithm can be given by $\mathcal{O}(L(2K+2E+5)^{3.5}+(2KN_t^2)^{3.5}+(2KM^2)^{3.5})$ according to [44], where L represents the number of iterations.

[2]Using the iterative algorithm, the proposed design can be extended to other cases with the knowledge of imperfect or statistic eavesdropping CSI.

Algorithm 1 Iterative Algorithm for Problem (21)

1: Initialization: Construct the initial feasible points $U_0^{(0)}$, $V_{0k}^{(0)}$, $S_{0k}^{(0)}$, $u_0^{(0)}$, $v_{0e}^{(0)}$, $T_{0e}^{(0)}$, $\mathbf{q}_{I0}^{(0)}$, $\mathbf{w}_k^{(0)}$ and $\mathbf{\Phi}^{(0)}$. Set the convergence threshold ε and the initial index $t=0$.
2: **Repeat**
3: With the given $\mathbf{W}_k$=$\mathbf{W}_k^{(t)}$ and $\mathbf{\Phi}=\mathbf{\Phi}^{(t)}$, solve the problem (34), and obtain $U_0^{(t+1)}$, $V_{0k}^{(t+1)}$, $S_{0k}^{(t+1)}$, $u_0^{(t+1)}$, $v_{0e}^{(t+1)}$, $T_{0e}^{(t+1)}$ and $\mathbf{q}_{I0}^{(t+1)}$.
4: Obtain $\mathbf{W}_k^{(t+1)}$ by solving the problem (43) with the given $\mathbf{\Phi}=\mathbf{\Phi}^{(t)}$ and the above results by solving the problem (34).
5: Set $\mathbf{V}^{(t)}$= $\mathrm{Diag}(\mathbf{\Phi}^{(t)})\ \mathrm{Diag}(\mathbf{\Phi}^{(t)})^H$.
6: Solve the problem (51) with the obtained $\mathbf{W}_k=\mathbf{W}_k^{(t+1)}$ and the value obtained in Step 3 to update $\mathbf{V}^{(t+1)}$.
7: Recover $\mathbf{v}^{(t+1)}$ from $\mathbf{V}^{(t+1)}$ and update $\mathbf{\Phi}^{(t+1)}$ = $\mathrm{diag}(\mathbf{v}^{(t+1)})$.
8: Update: $t=t+1$.
9: **Until** $\frac{(R_s^{(t)}-R_s^{(t-1)})}{R_s^{(t-1)}}\leq\varepsilon$.
10: Output: $\bar{\mathbf{C}}_I^{(t+1)}$, $\mathbf{W}_k^{(t+1)}$, $\mathbf{\Phi}^{(t+1)}$.

TABLE I
SIMULATION PARAMETERS

Legitimate user 1's coordinate	$\mathbf{q}_{k1}$=[80 m, 0 m, 0 m]$^{\mathrm{T}}$
Legitimate user 2's coordinate	$\mathbf{q}_{k2}$=[60 m, 10 m, 0 m]$^{\mathrm{T}}$
Center abscissa of eavesdropper 1	$x_{e1}\in[70\text{ m}, 85\text{ m}]$
Center abscissa of eavesdropper 2	$x_{e2}\in[85\text{ m}, 100\text{ m}]$
Center ordinate of eavesdroppers	$y_{e1}=y_{e2}=0$ m
Error of the radius	ε_e=10 m
Carrier frequency	2.4 GHz
Number of antennas N_t	4
Number of IRS reflecting elements M	16
Maximum transmit power	30 dBm
Channel power at d_0=1 m	-30 dB
Noise power	$\sigma_k^2=\sigma_e^2=-100$ dBm
Antenna separation	$d_1=d_2=\frac{\lambda}{2}$
Element spacing of IRS	$d_x=d_y=\frac{\lambda}{4}$
Constants of the specific environmental type	$a=11.95$, $b=0.14$
LoS probability threshold	$\varepsilon_{LoS}=0.9$

V. SIMULATION RESULTS

In this section, we evaluate the performance of the proposed scheme for the aerial IRS assisted secure wireless transmission via simulation results, where two legitimate users and two eavesdroppers are considered. Unless otherwise stated, the parameters are listed in Table I.

In Fig. 2, the convergence of the proposed algorithm for different number of IRS reflecting elements M is investigated. It can be observed that the iterative algorithm eventually converges when M is 16, 36 or 64. In particular, the algorithm converges more quickly with a smaller number of IRS

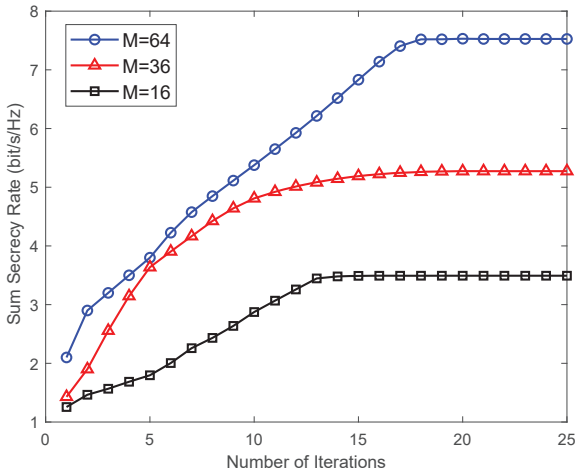

Fig. 2. Convergence of the proposed algorithm.

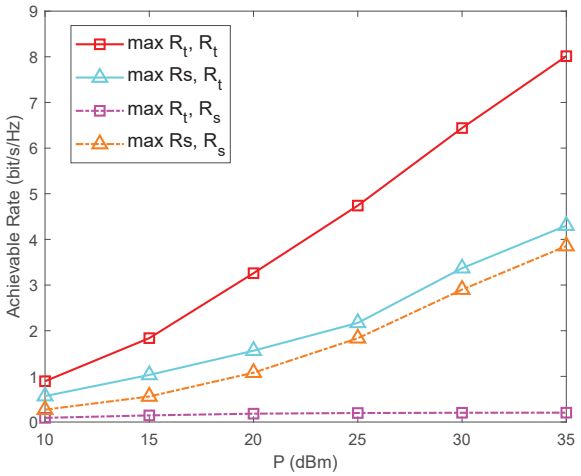

Fig. 4. Performance comparison between the proposed scheme and the sum transmission rate maximization scheme.

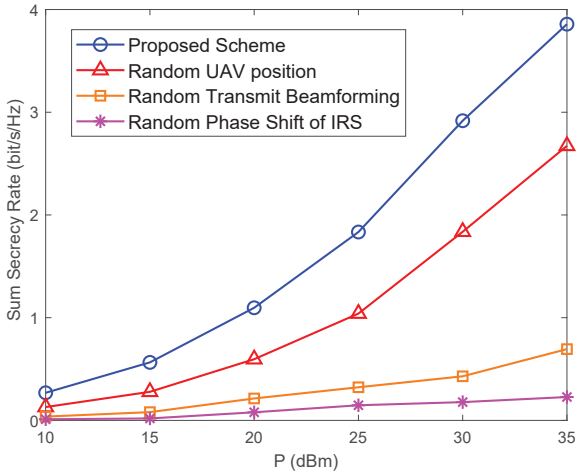

Fig. 3. Sum secrecy rate versus the transmit power for different benchmarks.

reflecting elements, e.g., about 15 iterations when $M = 16$. This is because the dimensions of the problem (20) increase with M. Furthermore, the sum secrecy rate becomes higher as the number of IRS reflecting elements increases.

In Fig. 3, we compare the proposed scheme with three benchmarks regarding the sum secrecy rate. The benchmark "Random UAV Position" indicates the transmit beamforming and passive beamforming design without optimizing the UAV position. The benchmark "Random Transmit Beamforming" denotes the UAV hovering position and passive beamforming design without optimizing the transmit beamforming. The benchmark "Random Phase Shifts of IRS" represents the UAV hovering position and transmit beamforming design without optimizing the phase shifts of IRS. From the results, we can see that the sum secrecy rate of these schemes all increases with the transmit power. Notably, the sum secrecy rate of the proposed scheme is far superior to that of all the benchmarks. Furthermore, the performance gap between the proposed scheme and these benchmarks tends to be wider when the transmit power P becomes higher. In addition, the benchmark "Random UAV Position" can achieve a higher sum secrecy rate than the other two benchmarks. Therefore, we can conclude that jointly optimizing the transmit beamforming, the phase shift of IRS and the hovering position of UAV can play a crucial role in improving the secure transmission performance.

To gain more insights, we compare the proposed scheme denoted by "max R_s" with the scheme denoted by "max R_t" that maximizes the sum transmission rate in Fig. 4. Specifically, we plot the sum secrecy rate and sum transmission rate versus the transmit power P. As can be observed, the sum transmission rate R_t increases with the transmit power for both the two schemes. As expected, the sum transmission rate maximization scheme achieves a higher sum rate than the proposed scheme due to their specific objective functions, and the gap enlarges with P. By contrast, the performance of the sum secrecy rate differs significantly between them. For the proposed scheme, it grows dramatically with rising P, while for the sum transmission rate maximization scheme, it keeps almost unchanged and close to zero. This illustrates that the proposed optimization scheme can suppress the eavesdropping effectively compared to the sum transmission rate maximization scheme.

Fig. 5 depicts the sum secrecy rate versus the number of reflecting elements. As the IRS consists of a UPA with $M = M_x M_y$ passive reflecting elements, we set $M_x = M_y$ for simplicity. As can be observed, the sum secrecy rate increases with M_x (M_y). Such a performance improvement is due to the increasing M. This means that more reflecting elements can receive the signal from AP, which leads to a larger passive beamforming gain. Furthermore, the results also show that equipping more antennas at AP can contribute to the security performance for the aerial IRS assisted wireless network. In summary, it can achieve a higher sum secrecy rate by jointly deploying more antennas and passive reflecting elements.

To further investigate the influence of the numbers of antennas and passive reflecting elements, we compare the sum secrecy rate R_s, the sum transmission rate R_t and the sum eavesdropping rate R_e in Fig. 6. The results show that the sum secrecy rate and the sum transmission rate increase as equipping more passive reflecting elements on the IRS. Besides,

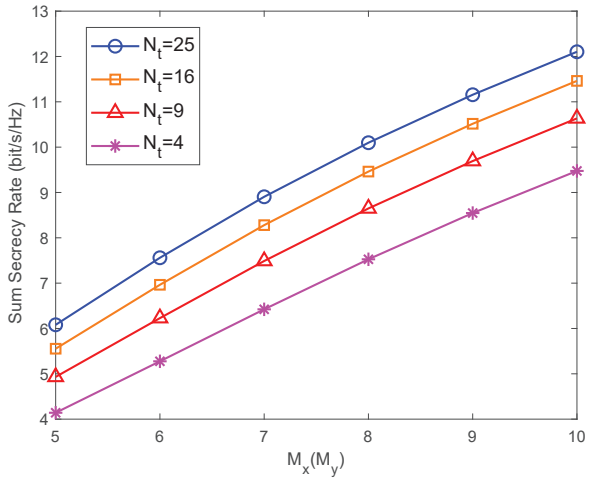

Fig. 5. Sum secrecy rate with different number of reflecting elements and antennas.

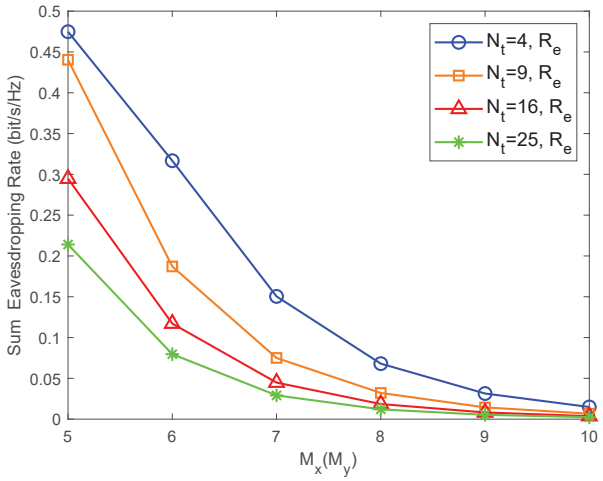

Fig. 7. Sum eavesdropping rate for all the legitimate users with different numbers of reflecting elements and antennas.

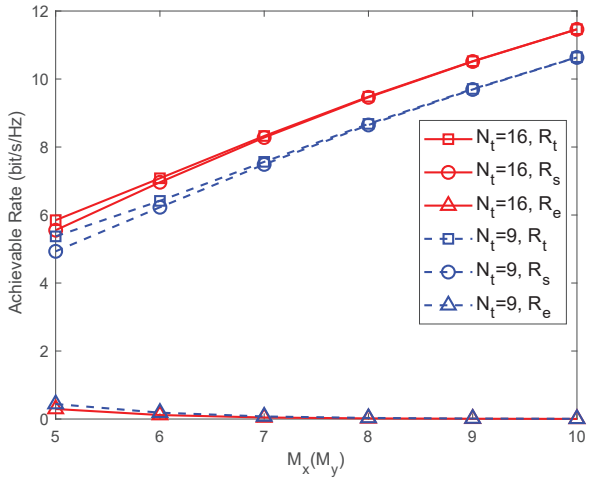

Fig. 6. Achievable rates versus the number of IRS reflecting elements with different numbers of antennas.

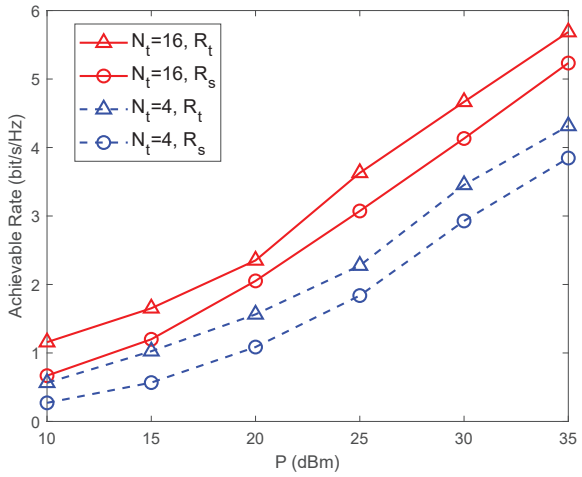

Fig. 8. Sum secrecy rate and sum transmission rate versus the transmit power of AP .

the gap between them narrows with M. Moreover, we can see from Fig. 6 that the sum eavesdropping rate decreases and tends to zero gradually with larger M. This result accounts for the reason why the gap between the sum secrecy rate and the sum transmission rate narrows. Thanks to the controllability of the phase shifts, the channels of legitimate users become better while the channels of eavesdroppers become worse as the reflecting elements increases. When the phase shifts are optimized properly, the received reflected signal power of the legitimate users increases while that of the eavesdroppers decreases. In addition, the sum secrecy rate and the sum transmission rate can be enhanced by increasing the number of antennas from 9 to 16. By contrast, we can observe from Fig. 7 that the sum eavesdropping rate decreases by increasing the number of transmit antennas. When equipping a large number of reflecting elements and transmit antennas, it can effectively suppress the eavesdropping and limit the information leakage to the potential eavesdroppers.

In Fig. 8, we present the sum secrecy rate and the sum transmission rate versus the transmit power P at AP with $N_t = 4$ and $N_t = 16$, respectively. As can be observed, the sum secrecy rate and the sum transmission rate increase monotonically with the transmit power P. This is because all the legitimate users can receive more signal power as P increases. The received signal-to-noise ratio (SNR) of the legitimate users can be enhanced by providing them with additional transmit power, which leads to a considerable performance improvement. Besides, the results show that the sum secrecy rate and the sum transmission rate can be enhanced effectively by equipping more antennas, which is consistent with the conclusions of Fig. 5.

In Fig. 9, we study the impact of the rate threshold on the rate performance. The result shows that the maximum transmission rate R_h among the legitimate users and sum secrecy rate R_s decreases with the rate threshold. This is because the feasible region shrinks by increasing the rate threshold of legitimate users. With the increase of the threshold, this constraint becomes more stricter and more difficult to satisfy. Thus, the sum secrecy rate and the maximum transmission rate among the legitimate users will be sacrificed to satisfy

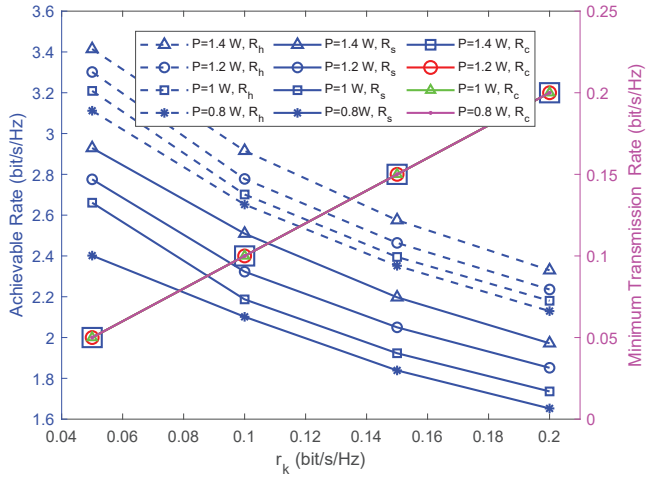

Fig. 9. Rate performance and the minimum transmission rate versus the rate threshold.

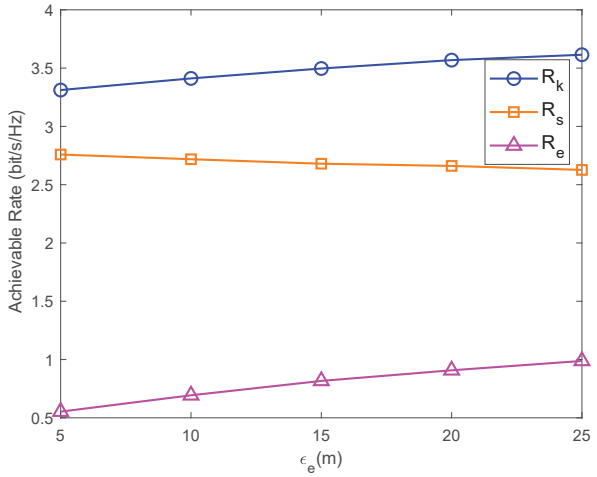

Fig. 10. Achievable rates versus the error of the radius ϵ_e.

the constraint. Conversely, the minimum transmission rate R_c among the legitimate users keeps unchanged with different transmit power and exactly equals to the minimum rate threshold. This is because after satisfying the minimum quality of service of a specific legitimate user, all the remaining resource will be allocated to other legitimate users to maximize the sum secrecy rate. In addition, by comparing the curves with different transmit power, we can conclude that increasing the power can contribute to the performance for the aerial IRS assisted secure transmission.

Fig. 10 illustrates the sum secrecy rate R_s, the sum transmission rate R_t and the sum eavesdropping rate R_e versus the error of the radius ϵ_e for the eavesdropper. As the error of the radius increases, less information can be obtained about the eavesdroppers, which will cause more serious information leakage. Thus, the sum eavesdropping rate increases with the radius ϵ_e. As the uncertainty of eavesdroppers location increases, the optimal UAV position will be closer to the legitimate users, and the sum transmission rate increases. However, the sum secrecy rate decreases with the radius error. This illustrates that the overall secrecy performance degrades as the estimation error ϵ_e increases.

VI. Conclusions

In this paper, aerial IRS has been investigated to achieve the secure communication in the presence of eavesdroppers whose accurate positions are unknown. Specifically, we jointly optimize the hovering position of UAV, the transmit beamforming of AP and the phase-shift matrix of IRS to maximize the worst-case sum secrecy rate. An AO algorithm is developed to solve the non-convex optimization problem. In particular, the hovering position optimization problem is transformed into a convex optimization by SCA. The beamforming optimization problems are first converted into rank-constrained problems by the SCA, and then solved by adopting the SDR. We resort to an iterative algorithm to solve these subproblems alternately until convergence. Numerical results verify the effectiveness of the proposed scheme and the significant secrecy performance gain achieved by the joint design. It's worth noting that several challenges, such as the accurate channel estimation and the training overhead, need to be addressed prior to the joint design. In our future work, we will continue to focus on the robust design for aerial IRS assisted wireless networks with imperfect eavesdropping CSI.

References

[1] W. Wei, X. Pang, N. Zhao, X. Wang, and A. Nallanathan, "Joint placement and precoding design for aerial IRS aided secure communication networks," *IEEE ICC'23*, pp. 1–6, accepted.

[2] C. Huang, S. Hu, G. C. Alexandropoulos, A. Zappone, C. Yuen, R. Zhang, M. D.Renzo, and M. Debbah, "Holographic MIMO surfaces for 6G wireless networks: Opportunities, challenges, and trends," *IEEE Wireless Commun.*, vol. 27, no. 5, pp. 118–125, Oct. 2020.

[3] Q. Wu and R. Zhang, "Towards smart and reconfigurable environment: Intelligent reflecting surface aided wireless network," *IEEE Commun. Mag.*, vol. 58, no. 1, pp. 106–112, Jan. 2020.

[4] H. Lu, Y. Zeng, S. Jin, and R. Zhang, "Aerial intelligent reflecting surface: Joint placement and passive beamforming design with 3D beam flattening," *IEEE Trans. Wireless Commun.*, vol. 20, no. 7, pp. 4128–4143, Feb. 2021.

[5] Q. Wu and R. Zhang, "Intelligent reflecting surface enhanced wireless network via joint active and passive beamforming," *IEEE Trans. Wireless Commun.*, vol. 18, no. 11, pp. 5394–5409, Nov. 2019.

[6] Q. Wu, S. Zhang, B. Zheng, C. You, and R. Zhang, "Intelligent reflecting surface-aided wireless communications: A tutorial," *IEEE Trans. Commun.*, vol. 69, no. 5, pp. 3313–3351, May 2021.

[7] D. Xu, X. Yu, Y. Sun, D. W. K. Ng, and R. Schober, "Resource allocation for IRS-assisted full-duplex cognitive radio systems," *IEEE Trans. Commun.*, vol. 68, no. 12, pp. 7376–7394, Dec. 2020.

[8] S. Gong, X. Lu, D. T. Hoang, D. Niyato, L. Shu, D. I. Kim, and Y.-C. Liang, "Toward smart wireless communications via intelligent reflecting surfaces: A contemporary survey," *IEEE Commun. Surveys Tuts.*, vol. 22, no. 4, pp. 2283–2314, 4th Quart. 2020.

[9] B. Zheng and R. Zhang, "IRS meets relaying: Joint resource allocation and passive beamforming optimization," *IEEE Wireless Commun. Lett.*, vol. 10, no. 9, pp. 2080–2084, Sept. 2021.

[10] T. Bai, C. Pan, Y. Deng, M. Elkashlan, A. Nallanathan, and L. Hanzo, "Latency minimization for intelligent reflecting surface aided mobile edge computing," *IEEE J. Sel. Areas in Commun.*, vol. 38, no. 11, pp. 2666–2682, Nov. 2020.

[11] Y. Mi and Q. Song, "Energy efficiency maximization for IRS-aided WPCNs," *IEEE Wireless Commun. Lett.*, vol. 10, no. 10, pp. 2304–2308, Oct. 2021.

[12] Q. Wu and R. Zhang, "Intelligent reflecting surface enhanced wireless network via joint active and passive beamforming," *IEEE Trans. Wireless Commun.*, vol. 18, no. 11, pp. 5394–5409, Nov. 2019.

[13] X. Pang, N. Zhao, J. Tang, C. Wu, D. Niyato, and K.-K. Wong, "IRS-assisted secure UAV transmission via joint trajectory and beamforming design," *IEEE Trans. Commun.*, vol. 70, no. 2, pp. 1140–1152, Feb. 2022.

[14] Y.-S. Shiu, S. Y. Chang, H.-C. Wu, S. C.-H. Huang, and H.-H. Chen, "Physical layer security in wireless networks: a tutorial," *IEEE Wireless Commun.*, vol. 18, no. 2, pp. 66–74, Apr. 2011.

[15] X. Chen, C. Zhong, C. Yuen, and H.-H. Chen, "Multi-antenna relay aided wireless physical layer security," *IEEE Commun. Mag.*, vol. 53, no. 12, pp. 40–46, Dec. 2015.

[16] W. Zhang, J. Chen, Y. Kuo, and Y. Zhou, "Artificial-noise-Aided optimal beamforming in layered physical layer security," *IEEE Commun. Lett.*, vol. 23, no. 1, pp. 72–75, Jan. 2019.

[17] F. Zhu and M. Yao, "Improving physical-layer security for CRNs using SINR-Based cooperative beamforming," *IEEE Trans. Veh. Technol.*, vol. 65, no. 3, pp. 1835–1841, Mar. 2016.

[18] G. C. Alexandropoulos, K. D. Katsanos, M. Wen, and D. B. d. Costa, "Counteracting eavesdropper attacks through reconfigurable intelligent surfaces: A new threat model and secrecy rate optimization," *arXiv e-prints*, arXiv:2212.02263, Dec. 2022.

[19] W. Jiang, B. Chen, J. Zhao, Z. Xiong, and Z. Ding, "Joint active and passive beamforming design for the IRS-assisted MIMOME-OFDM secure communications," *IEEE Trans. Veh. Technol.*, vol. 70, no. 10, pp. 10369–10381, Oct. 2021.

[20] S. Hong, C. Pan, H. Ren, K. Wang, and A. Nallanathan, "Artificial-noise-aided secure MIMO wireless communications via intelligent reflecting surface," *IEEE Trans. Commun.*, vol. 68, no. 12, pp. 7851–7866, Dec. 2020.

[21] H. Yang, Z. Xiong, J. Zhao, D. Niyato, L. Xiao, and Q. Wu, "Deep reinforcement learning-based intelligent reflecting surface for secure wireless communications," *IEEE Trans. Wireless Commun.*, vol. 20, no. 1, pp. 375–388, Jan. 2021.

[22] Y. Zeng, R. Zhang, and T. J. Lim, "Wireless communications with unmanned aerial vehicles: opportunities and challenges," *IEEE Commun. Mag.*, vol. 54, no. 5, pp. 36–42, May 2016.

[23] W. Feng, J. Wang, Y. Chen, X. Wang, N. Ge, and J. Lu, "UAV-aided MIMO communications for 5G internet of things," *IEEE Internet Things J.*, vol. 6, no. 2, pp. 1731–1740, Apr. 2019.

[24] A. Masaracchia, L. D. Nguyen, T. Q. Duong, C. Yin, O. A. Dobre, and E. Garcia-Palacios, "Energy-efficient and throughput fair resource allocation for TS-NOMA UAV-assisted communications," *IEEE Trans. Commun.*, vol. 68, no. 11, pp. 7156–7169, Nov. 2020.

[25] A. A. Al-Habob, O. A. Dobre, S. Muhaidat, and H. Vincent Poor, "Energy-efficient data dissemination using a UAV: An ant colony approach," *IEEE Wireless Commun. Lett.*, vol. 10, no. 1, pp. 16–20, Jan. 2021.

[26] N. Liu, X. Tang, R. Zhang, D. Wang, and D. Zhai, "A DNN framework for secure transmissions in UAV-relaying networks with a jamming receiver," in *Proc. IEEE ICCT*, pp. 703–708, Nanning, China, Oct. 2020.

[27] C. Zhong, J. Yao, and J. Xu, "Secure UAV communication with cooperative jamming and trajectory control," *IEEE Commun. Lett.*, vol. 23, no. 2, pp. 286–289, Feb. 2019.

[28] X. Chen, D. Li, Z. Yang, Y. Chen, N. Zhao, Z. Ding, and F. R. Yu, "Securing aerial-ground transmission for NOMA-UAV networks," *IEEE Netw.*, vol. 34, no. 6, pp. 171–177, Nov. 2020.

[29] X. Pang, M. Sheng, N. Zhao, J. Tang, D. Niyato, and K.-K. Wong, "When UAV meets IRS: Expanding air-ground networks via passive reflection," *IEEE Wireless Commun.*, vol. 28, no. 5, pp. 164–170, Oct. 2021.

[30] Z. Wei, Y. Cai, Z. Sun, D. W. K. Ng, J. Yuan, M. Zhou, and L. Sun, "Sum-rate maximization for IRS-assisted UAV OFDMA communication systems," *IEEE Trans. Wireless Commun.*, vol. 20, no. 4, pp. 2530–2550, Apr. 2021.

[31] L. Ge, P. Dong, H. Zhang, J.-B. Wang, and X. You, "Joint beamforming and trajectory optimization for intelligent reflecting surfaces-assisted UAV communications," *IEEE Access*, vol. 8, pp. 78702–78712, 2020.

[32] C. Wang, X. Chen, J. An, Z. Xiong, C. Xing, N. Zhao, and D. Niyato, "Covert communication assisted by UAV-IRS," *IEEE Trans. Commun.*, vol. 71, no. 1, pp. 357–369, Jan. 2023.

[33] Y. Su, X. Pang, S. Chen, X. Jiang, N. Zhao, and F. Richard Yu, "Spectrum and energy efficiency optimization in IRS-assisted UAV networks," *IEEE Trans. Commun.*, to appear.

[34] H. Niu, Z. Chu, Z. Zhu, and F. Zhou, "Aerial intelligent reflecting surface for secure wireless networks: Secrecy capacity and optimal trajectory strategy," *Intell. Converged Netw.*, vol. 3, no. 1, pp. 119–133, Mar. 2022.

[35] X. Xie and G. Lu, "A research of object detection on UAVs aerial images," in *2021 ICBASE*, pp. 342–345, Zhuhai, China, Sept. 2021.

[36] M. Mozaffari, W. Saad, M. Bennis, and M. Debbah, "Unmanned aerial vehicle with underlaid device-to-device communications: Performance and tradeoffs," *IEEE Trans. Wireless Commun.*, vol. 15, no. 6, pp. 3949–3963, Jun. 2016.

[37] M. Jian, G. C. Alexandropoulos, E. Basar, C. Huang, R. Liu, Y. Liu and C. Yuen, "Reconfigurable intelligent surfaces for wireless communications: Overview of hardware designs, channel models, and estimation techniques," *ITU Intell. Converged Netw.*, vol. 3, no. 1, pp. 1–32, 2022.

[38] L. Wei, C. Huang, G. C. Alexandropoulos, C. Yuen, Z. Zhang, and M. Debbah, "Channel estimation for RIS-empowered multi-user MISO wireless communications," *IEEE Trans. Commun.*, vol. 69, no. 6, pp. 4144–4157, Jun. 2021.

[39] M. T. Mamaghani and Y. Hong, "Improving PHY-security of uav-enabled transmission with wireless energy harvesting: Robust trajectory design and communications resource allocation," *IEEE Trans. Veh. Technol.*, vol. 69, no. 8, pp. 8586–8600, Aug. 2020.

[40] C. Huang, A. Zappone, G. C. Alexandropoulos, M. Debbah, and C. Yuen, "Reconfigurable intelligent surfaces for energy efficiency in wireless communication," *IEEE Trans. Wireless Commun.*, vol. 18, no. 8, pp. 4157–4170, Aug. 2019.

[41] X. Yu, D. Xu, Y. Sun, D. W. K. Ng, and R. Schober, "Robust and secure wireless communications via intelligent reflecting surfaces," *IEEE J. Sel. Areas Commun.*, vol. 38, no. 11, pp. 2637–2652, Jul. 2020.

[42] A. M.-C. So, J. Zhang and Y. Ye, "On approximating complex quadratic optimization problems via semidefinite programming relaxations," *Mathematical Programming*, vol. 110, no. 1, pp. 93–110, Jun. 2007.

[43] Z. Li, W. Chen, Q. Wu, K. Wang, and J. Li, "Joint beamforming design and power splitting optimization in IRS-assisted SWIPT NOMA networks," *IEEE Trans. Wireless Commun.*, vol. 21, no. 3, pp. 2019–2033, Mar. 2022.

[44] G. Zhang, Q. Wu, M. Cui, and R. Zhang, "Securing UAV communications via joint trajectory and power control," *IEEE Trans. Wireless Commun.*, vol. 18, no. 2, pp. 1376–1389, Feb. 2019.